Numerical Models of Two Complex Hypersonic Flowfields

M. G. Macaraeg*
NASA Langley Research Center, Hampton, Virginia

Numerical solutions of the compressible Navier-Stokes equations assuming a perfect gas and laminar flow are applied to two hypersonic experiments conducted at NASA Langley Research Center. The first is cooling by injection of a gas jet through the nose of an ogive-cone, and the second is the aerothermal environment in the gap formed by the wing and elevon section of a test model of the Space Shuttle. The simulations demonstrate that the model predicts accurate pressures and shock stand-off for the gas jet and accurate pressures for the wing-elevon cove. Experimental heating rates for the gas jet indicate turbulent mixing to be occurring, an effect not modeled in the numerical solution.

Introduction

In recent years an increased interest in hypersonic vehicle concepts has brought a number of aerodynamic problems for hypersonic flow into prominence. These problems are characterized by high-temperature high-velocity flows with strong viscous interactions. A dominant feature of these flows is the aerodynamically induced high heat transfer rates to the vehicle surfaces. Accurate heat transfer rates are difficult to obtain numerically and difficult to measure experimentally. However, accurate heating rates are important when designing a given structure and assessing its reliability.

Numerical and experimental models are important tools for understanding the aerothermal environment in high-speed flows. However, before extrapolating the results of such models to actual flight conditions careful model validation along with an understanding of the effects model assumptions have on the simulated physics are important first steps.

This paper will present results from numerical models of two experiments investigated at NASA Langley Research Center.[1] The studies were undertaken to complement experimental results by providing detailed information not obtainable experimentally. The solution technique is a second-order-accurate Beam and Warming alternating direction implicit (ADI) algorithm.[2] The algorithm is augmented to include an explicit blend of second and fourth differences for the dissipative terms.[3]

The first problem is Mach 6.7 flow over a gas-jet-cooled ogive cone [gas jet nose tip (GJNT); see Fig. 1a]. Protecting a nose tip from severe thermal and pressure environments is an important concern for advanced entry vehicles. Very little experimental or numerical results exist for high-enthalpy hypersonic flow conditions for GJNT on large cones. Therefore, a test program was conducted in the Langley 8-ft High Temperature Tunnel (8-ft HTT) to study mass addition cooling by GJNT.[4,5] Numerical shock stand-off distances, pressures, and cold wall heating rates will be compared to experimental results.

The second problem, studied in only a preliminary fashion, is the determination of the fluid/thermal environment in the cove between the Space Shuttle wing and elevon surfaces (Fig. 1b) that has been a concern throughout the design and initial operational phases of the vehicle. If the seals at the elevon hinge line leak, hot boundary-layer gas flowing into the cove will endanger the thermally unprotected inner wing and elevon structures. Previous attempts using finite-difference techniques[6] were unable to obtain quantitative results, possibly due to difficulties encountered with modeling the complex geometry. Finite-element techniques have handled the geometric complexity, and solutions have been obtained for both incompressible flow in the cove only[7] and for inviscid flow for the external and internal flowfields.[8] However, since details of the flow at the mouth and internal to the cove will be dominated by viscous effects and the shear layer emanating from the rear of the wing panel, a full Navier-Stokes solution is required. The numerical analysis to be given models the flow with the viscous-compressible Navier-Stokes equations. Comparison of results with data from a full-scale model for the wing-elevon cove tested in the 8-ft HTT[9] is also given.

Numerical Model

The governing equations are the viscous, compressible Navier-Stokes equations as given in Refs. 10 and 11. The model assumes a perfect gas and laminar flow. The Prandtl number and ratio of specific heats are held constant. The coefficient of thermal conductivity and the first coefficient of viscosity are calculated from Sutherland's law.[12] The second coefficient of viscosity is obtained from Stokes' law.[12]

The finite-difference solution technique is a second-order-accurate Beam and Warming ADI algorithm. The algorithm is augmented to include an adaptive blend of second and fourth differences for the dissipative terms regulated by the pressure gradient in the local flowfield. Their addition controls the odd-even uncoupling of grid points typical of central-difference schemes and provides strong dissipation in the region of shock waves and lesser dissipation in the remainder of the field. Details of the numerical scheme are given in Ref. 11.

All calculations were performed on the Langley CYBER 175 and took 0.00247 s/pt./iteration of CPU time.

Gas Jet Nose Tip

Nonblowing Test Cases

Before modeling the GJNT, a series of cases for blunted cones without gas injection were studied to assess the effects that convergence, resolution, and artificial dissipation have on numerical results without the added complications of the gas jet.[11] The numerical results were compared with experiments of Mach 6.7 flow over conical bodies conducted in the 8-ft HTT.[13] The study demonstrated that accurate pressure calculations are easily obtained on a coarse grid, with convergence being obtained after the residual decreases by four orders of magnitude. However, accurate heating rates require a fine-grid solution with convergence requiring at least a reduction of six orders of magnitude in the residual. The effect of artificial dissipation on

Presented as Paper 86-0234 at the AIAA 24th Aerospace Sciences Meeting, Jan. 6–9, 1986, Reno, NV; received Jan. 6, 1987; revision. Received Sept. 16, 1987.

*Research Scientist, Computational Methods Branch, High Speed Aerodynamics Division. Member AIAA.

numerical results is also assessed. Details of this study are given in Ref. 11. Subsequent work has revealed that approximately 15–20 grid points are needed in the boundary layer to obtain stagnation-point heating rates within 5.5% of experimental data. A second-order one-sided difference formula was utilized to obtain this value. The grid (35 points along the body, 51 normal to the body) is exponentially stretched in the normal direction to improve resolution of the boundary layer. This results in relatively large grid spacing near the shock, but the study showed that the shock jump conditions were relatively insensitive to resolution. There is also a stretching in the tangential direction to resolve the expanding flow around the hemispherical nose.

Gas Jet Nose Tip

To reduce the excessive heating loads on bodies in hypersonic flow a study of the cooling effectiveness produced by mass injection was conducted in the 8-ft HTT.[4,5] A parallel study is presented using the Navier-Stokes code. Freestream conditions are $M_\infty = 6.7$, $\gamma = 1.382$, Prandtl number $= 0.743$; the Reynolds number was 9.33×10^4 based on nozzle-exit radius. The gas jet has a temperature of 275 K and is sonic at the outlet. The total pressure of the coolant divided by the pitot pressure of the flow is 2.46, producing an underexpanded jet of coolant gas. These conditions are the same as tunnel test conditions. However, the experiment is in a test medium of combustion products of methane and air and the gas jet is nitrogen, while the numerical model assumes perfect gas relations and ignores molecular diffusion. Since reasonable agreement between experimental and perfect-gas numerical heating rates was obtained for the nonblowing cases, however, the secondary effect of molecular diffusion was considered negligible for this study.

Numerical results are obtained on a 35×41 grid (35 points along the body and 41 normal to the body) as given in Fig. 2. The grid is exponentially stretched in the normal direction, although less severely than the nonblowing cases, and there is also a stretching applied in the tangential direction. Convergence is assumed after the residual is reduced to six orders of magnitude.

In 1965 GJNT experiments conducted by Finley[14] on a blunter body led him to postulate flow features based on schlieren, shadowgraph, and experimental data. A schematic taken from Ref. 14 is reproduced in Fig. 3. The schematic depicts a low-velocity recirculation zone surrounded by a shear or mixing layer that attaches to the body beyond the recircula-

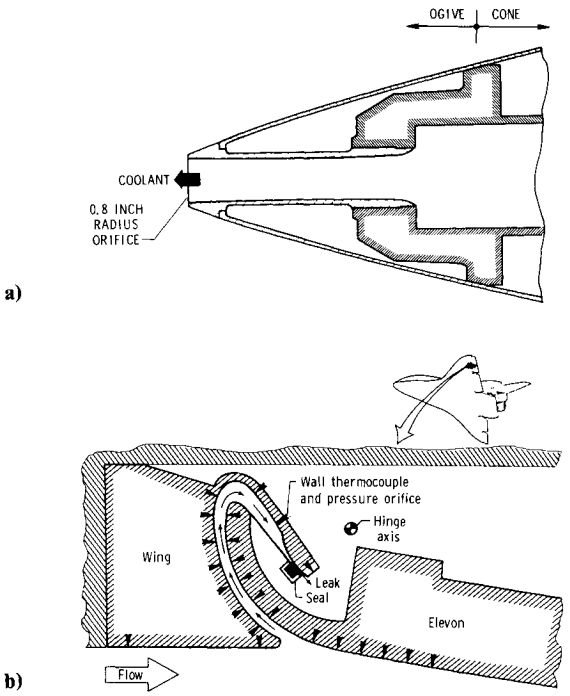

Fig. 1 Tests in the 8-ft High Temperature Tunnel at NASA Langley Research Center: a) gas jet nose-tip ogive-cone; b) wing-elevon cove.

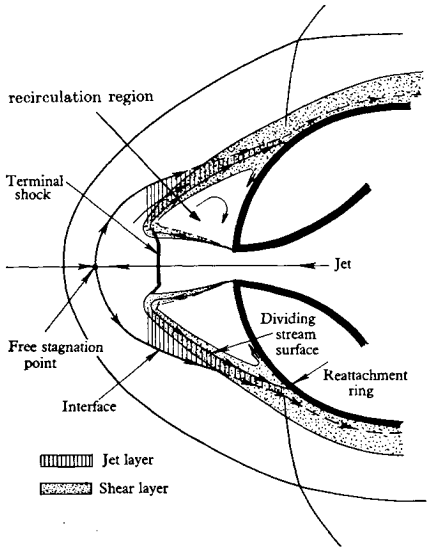

Fig. 3 Features of a GJNT flowfield (Ref. 14).

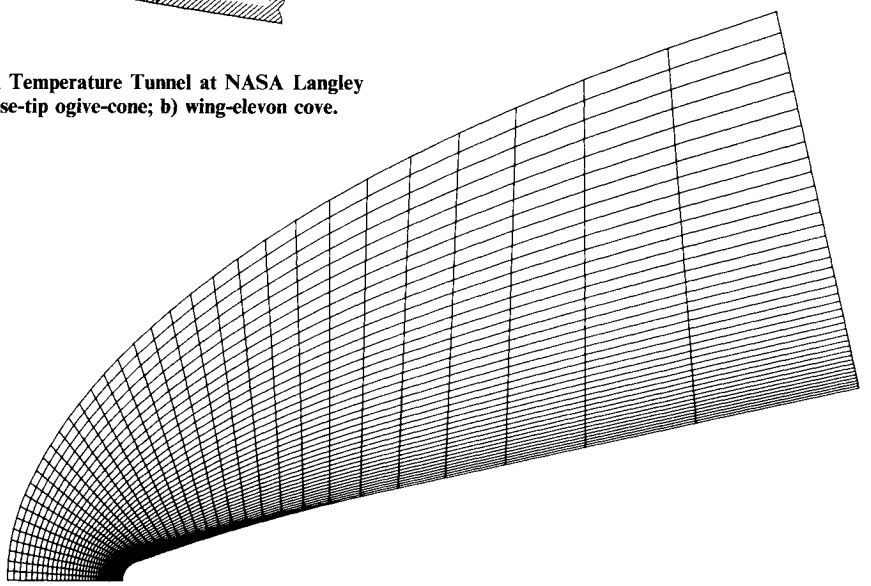

Fig. 2 Computational grid for GJNT solution.

tion zone. A comparison between GJNT experiments conducted in the 8-ft HTT and the numerical model reveals similar features.

Figure 4 is a qualitative comparison of shock stand-off distance that interfaces a shadowgraph from the GJNT experiment[4] with Mach number contours from the numerical solution. The experimental stand-off distance compares well with the low Mach number part of the simulated shock. Studies in Ref. 11 show that a finer grid will cause the numerical shock to steepen up toward the low Mach number side. A quantitative plot of shock stand-off distance vs angular distance about the symmetry line at the nozzle-exit plane is given in Fig. 5. The stand-off distance is measured along a ray from the point of intersection of the nozzle-exit plane and the axis symmetry to the shock. All distances presented for this configuration are nondimensionalized by the nozzle-exit radius.

Figure 6 is a plot of temperature contours ($T_w = 300$ K) that helps illustrate some important flow features. The distance indicated as $s = 10.2$ cm (axial) encompasses a recirculation region (that is confirmed by numerical values of velocities) where the cold gas is most effective in cooling the body. Downstream of this recirculation zone, at approximately 10.2 cm from the nose tip, flow reattaches and the temperature contours move in toward the body, although a cold layer of gas still persists down the length of the body. Heating rates remain negative outside the recirculation region but increase after the recirculation zone. The separation and attachment point as well as the recirculation zone are more easily seen in Fig. 7, which depicts flow-direction arrows in this region. Some of these same features are revealed by image enhancements of experimental photographs. Figure 8 is a color image enhancement of a schlieren taken of a GJNT experiment.[5] The color contrasts help delineate the recirculation region and an outer mixing of hot incoming gas mixing with the jet and impinging on the body downstream of this recirculation zone.

Figure 9 is a composite of two enhancements of the shadowgraph in Fig. 4. It shows further detail of the recirculating gas jet and depicts a turbulent mixing layer outside the recirculation region. Experimental heat transfer data also indicates turbulent mixing to be occurring. These observations are not surprising since the Reynolds number of the gas jet based on the nozzle diameter is approximately 2×10^6, which is three orders of magnitude higher than the Reynolds number for fully developed turbulent pipe flow.

Figure 10 is a comparison of numerical and experimental cold wall ($T_w = 300$ K) heating rates. These heating rates are nondimensionalized by a stagnation-point value from a non-

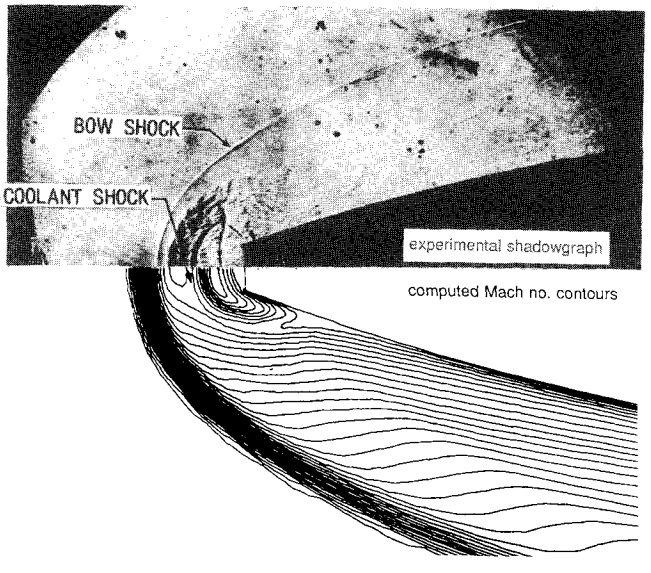

Fig. 4 Qualitative comparison of numerical and experimental models of the GJNT.

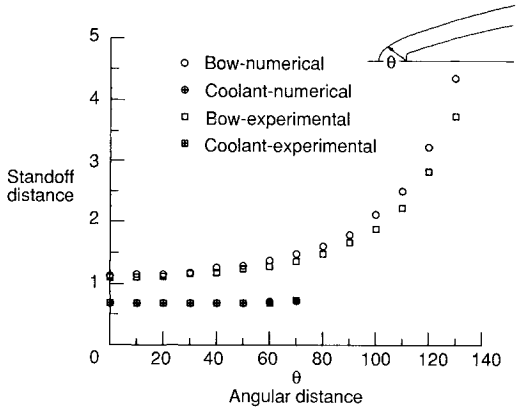

Fig. 5 Comparison of numerical and experimental shock stand-off distances for GJNT.

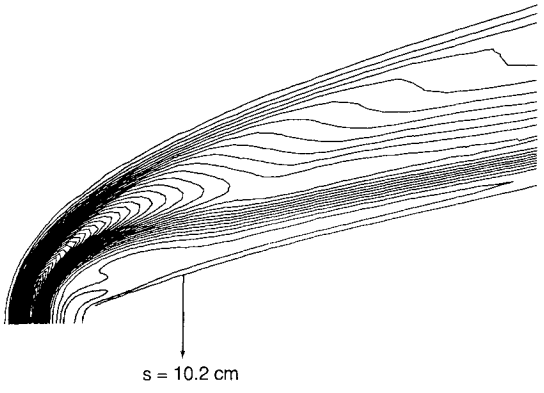

Fig. 6 Temperature contour plot of GJNT.

blowing experimental case. The heating in the numerical model is due to lateral conduction as expected in a laminar flow. The experimental data show high positive heating rates downstream of the recirculation zone indicating turbulent mixing of the hot incoming gas with the turbulent gas jet. Note that experimental heating rates radically increase at approximately 10.2 cm from the nose tip, which is the length of the recirculation region indicated in the temperature contour plot of Fig. 6. However, the numerical heating rates remain negative downstream of the recirculation zone.

Figures 11 and 12 reveal that differences in gas jet temperatures are not sufficient to account for the discrepancy between numerical and experimental heat transfer. The numerical results for an adiabatic case (Fig. 11) show adiabatic wall temperatures below the cold wall temperature 300 K, which confirm the negative heating rates in Fig. 10. Figure 11 is a plot of adiabatic wall temperatures for the cold gas jet (275 K) and a slightly warmer gas jet (300 K). The adiabatic temperatures are well below the fixed cold wall temperature, the warmer gas having slightly higher adiabatic temperatures. As expected, a warmer gas results in higher heating rates as shown in Fig. 12, which plots heating rates for gas jets of 275 and 445 K. However, since the increase in heating rates is small for a 170 K rise in gas jet temperature, differences in gas jet temperature are not sufficient to account for discrepancies between numerical and experimental heating rates.

In Fig. 13 numerical and experimental heat transfer comparisons are presented for a gas jet with a blowing pressure ratio of 5.05, approximately twice the value of the previous case. Good agreement with experimental data persists roughly twice the distance ($s = 20.4$ cm) as the lower pressure ratio case. Note the trend exhibited by the experimental data, however. The experimental heat transfer rises approximately linearly between 3 and 9 nose radii, then abruptly changes slope and rises much faster thereafter. It is conjectured that this change in slope is indicative of the onset of transition; appar-

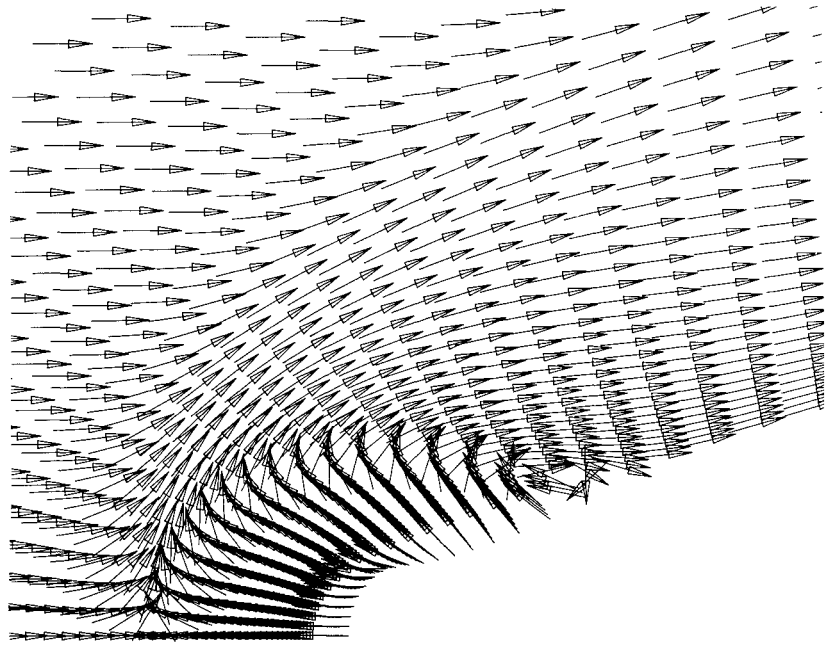

Fig. 7 Flow-direction plot in recirculation region of the GJNT.

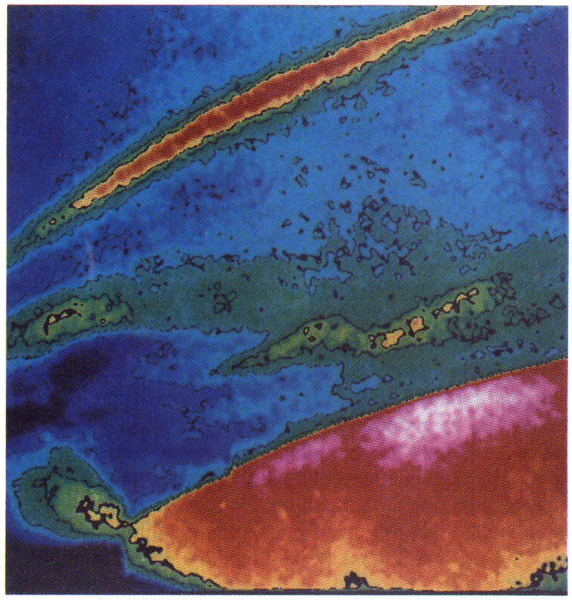

Fig. 8 Image enhancement of GJNT schlieren.

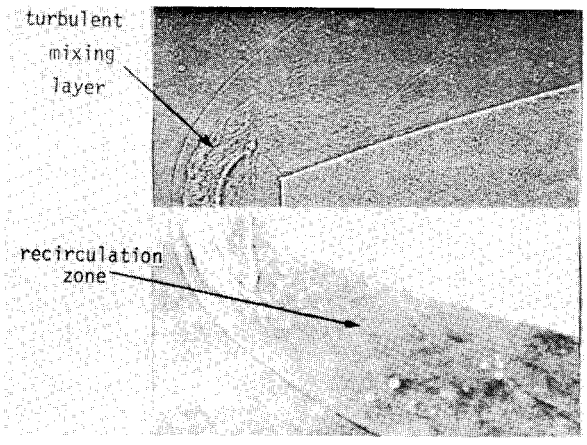

Fig. 9 Image enhancement of GJNT shadowgraph.

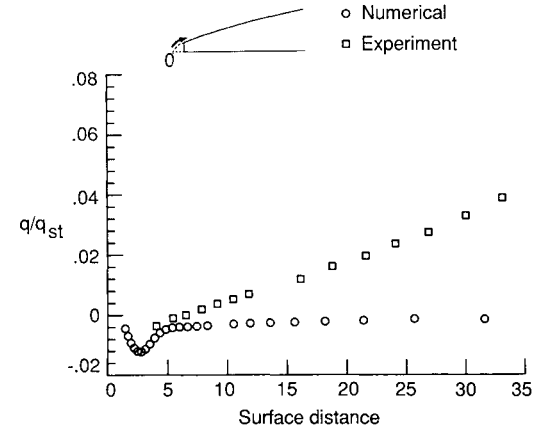

Fig. 10 Calculated and experimental cold wall heating rates for GJNT (blowing pressure ratio = 2.46).

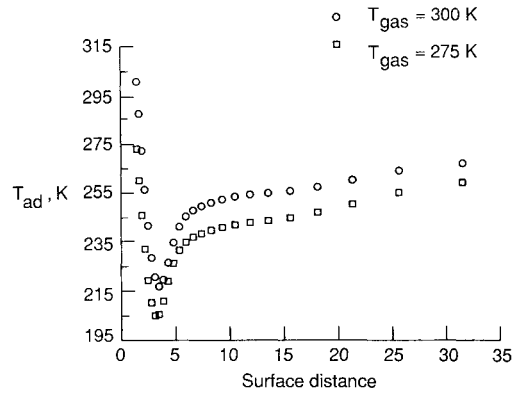

Fig. 11 Calculated adiabatic temperatures for GJNT.

ently, the higher blowing mass flow moved the transition downstream relative to the previous, lower mass flow case. Agreement of the numerical model with the data is good in the region before the apparent transition point. These observations imply that the elevated heating rates of the experiment are a

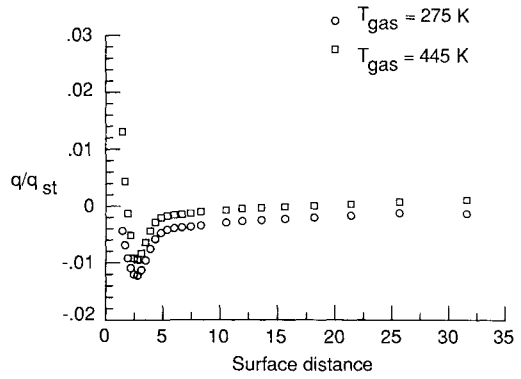

Fig. 12 Effect of gas jet temperature for GJNT.

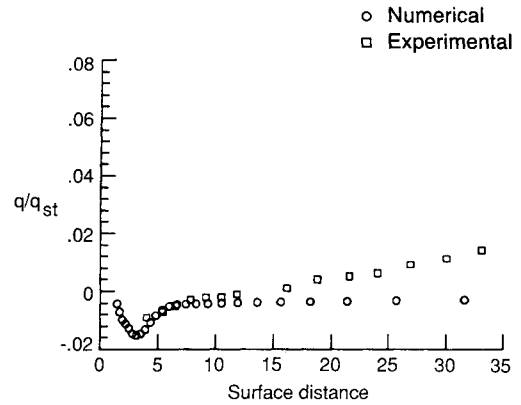

Fig. 13 Calculated and experimental cold wall heating rates for GJNT (blowing pressure ratio = 5.05).

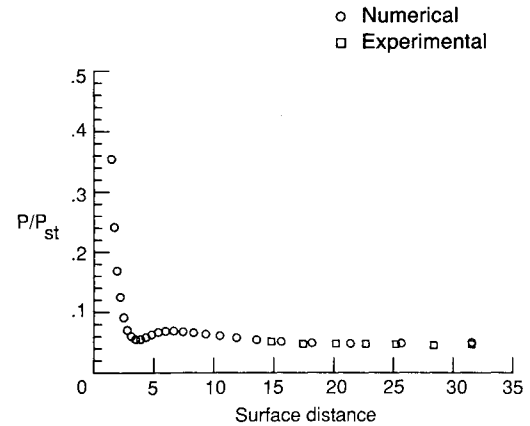

Fig. 14 Calculated and experimental pressure for GJNT.

consequence of a transitional boundary layer. The numerical comparisons with experiment also suggest that maintaining the gas jet as laminar as possible will increase its cooling effectiveness. For example, if the gas jet issued forth from a converging nozzle, large-scale turbulence might be substantially reduced so that viscosity could effectively dissipate the now small-scale turbulence.

Comparison of experimental[4] and numerical pressures normalized by the stagnation point value for a nonblowing case is given in Fig. 14. The numerical pressures indicate a dip in the recirculating region. Experimental data begin outside of this region at approximately 30.5 cm. The comparison indicates good agreement. A calculation of the ratio between the pressure behind the normal shock and P_∞ for a nonblowing case is 57.702. The highest pressure ratio in the GJNT numerical model, experienced at the lip of the ogive, is around 31. Thus, the gas jet substantially reduces the pressure load on the nose tip.

Preliminary Study of a Wing-Elevon Cove

The last problem to be addressed is a study of the fluid/thermal environment in the cove between the wing and elevon on the Space Shuttle (Fig. 1b). The gap between the Space Shuttle wing and elevon surface is closed by seals at the elevon hinge line to prevent the leakage of hot boundary-layer gases. If these hot gases flow into the cove, damage to the thermally unprotected inner wing and elevon structures could occur. To provide insight into the problem, a full-scale model of the wing-elevon cove was tested in the 8-ft HTT.[9] A two-dimensional Navier-Stokes solution of the aerothermal environment of the wing-elevon cove is given. A major difficulty in obtaining a reliable numerical solution had been producing a computational grid that models the cove geometry adequately. A fully interactive two-dimensional algebraic grid generator,[15] developed by Erlebacher at Langley, is used to generate the grid required for the present work. Figure 15a shows the grid produced by this method for a cove geometry in which the seal "leak" area is equal to the entrance area and the elevon deflection is 25 deg with respect to the wing. The grid is composed of 55 points on the coordinate family that spans the cove gap and 81 points on the opposite family. The entrance "neck" region is quite difficult to grid with adequate resolution and near-orthogonality; the enlargement of that region shown in Fig. 15b shows good performance by the above procedure.

In the experimental investigation of the configuration the elevon/gap apparatus was mounted in a flat test bed inserted into the tunnel; a flat run of approximately 1.22 m preceded the

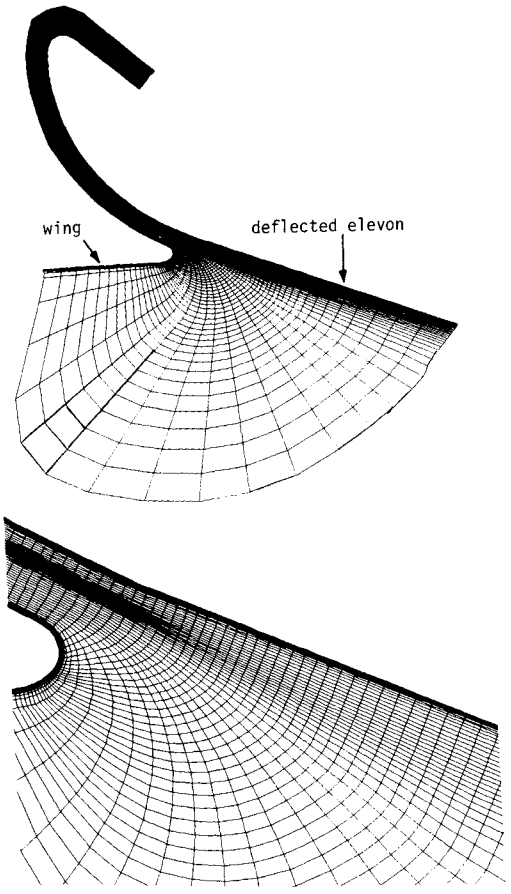

Fig. 15 Grid system for wing-elevon cove problem: a) entire computational domain; b) expanded portion of the "neck" region.

cove entrance. The entire test bed was inclined 5 deg (compression) with respect to freestream. The tunnel freestream conditions were $M_\infty = 6.7$, $T_\infty = 222$ K, and the Reynolds number based on cove entrance gap was 115,000.

Upstream inflow conditions were difficult to set in the numerical model, since the inclination of the experimental apparatus resulted in a weak shock with a slight entropy layer due to the small-radius (3/8 in.) leading edge. Since no detailed surveys of the flowfield upstream of the cove are available, numerical inflow conditions were approximated by setting tunnel freestream conditions inclined at 5 deg to the wing surface, blending to a flat-plate boundary-layer profile near the wing surface. The thickness of the boundary layer was about 20% of the cove entrance gap, consistent with the flat plate run preceding the cove entrance in the experimental apparatus. The effect of these approximate inflow conditions requires further assessment. No-slip, flow tangency, and zero-pressure gradient were imposed on the wing and elevon surfaces, along with either adiabatic (zero normal-temperature gradient) or constant wall temperature (300 K) conditions. Extrapolation was used at both freestream outflow and cove "leak" regions. It is interesting to note that the extrapolation condition in the "leak" region where the flow is subsonic had no effect on the numerical results. The extrapolated value pressure in the model was found to match the experimental value of Ref. 9. An imposed value of experimental pressure at the outflow leak region in the numerical model was also tested. No change was found between numerical results using either outflow condition.

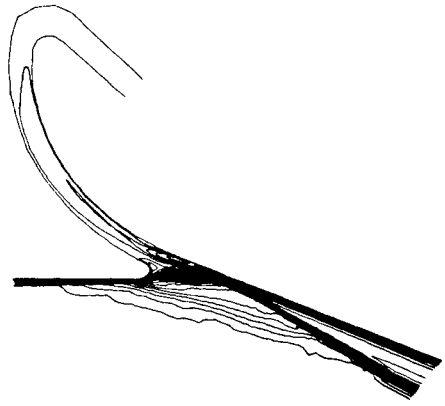

Fig. 16 Mach number contours of the wing-elevon cove.

Figure 16 is a Mach number contour plot of the flow in the wing-elevon cove. Note the weak compression waves upstream of the cove entrance due to the 5 deg angle of the input conditions, as mentioned previously. Since the leading edge is 1.22 m from the cove entrance in the experiment, the compression waves did not have a comparable impact on the flow in the near vicinity of the cove entrance. The boundary layer separates from the wing trailing edge, forming a shear layer across the cove entrance that impinges on the deflected elevon downstream where the elevon shock forms. Separation occurs just upstream of the cluster of flow-direction arrows at the wing trailing edge in Fig. 17 indicating a reversal of flow direction. On the cove side of the shear layer a large primary recirculation region forms and flow is directed into the cove. A small secondary recirculating area appears on the elevon surface inside of the cove. In Fig. 17 this secondary vortex is seen as the flow initially heads up the cove and then abruptly reverses direction in a confined region above the recirculation. The plot of density given in Fig. 18 characterizes the primary recirculation as a region of low density. The primary recirculation is quite strong; local Mach numbers exceed 1 in some areas. However, little flow is induced farther up the cove where Mach numbers are less than 0.3. These quantitative features are shown in Fig. 19, which is a plot of Mach number. Note the two very distinct regions of flow: the high Mach number flow in the freestream as opposed to the gases in the cove delineated by the shear layer that spans the mouth of the cove. In Fig. 20 regions of high temperature are seen on the wing and elevon boundary layers and in the recirculation area. The primary recirculation confines a region of high temperature; in the cove remain relatively low. The plot of enthalpy in Fig. 21 shows the very low energy gases in this recirculation zone and in the entire cove area. Note, again, the shear layer that extends across the cove entrance. This shear layer effectively shields the gases in the cove from the freestream. The combination of low density (Fig. 18) and enthalpy in the cove yields little heat load for this particular case of freestream Mach number, angle of attack, and flap angle.

Comparisons are made with experimental data in Fig. 22 for the pressure coefficient C_p vs surface distance. The distance is normalized by the cove entrance gap. As indicated in this figure, measurements begin at 0 in the cove and proceed down

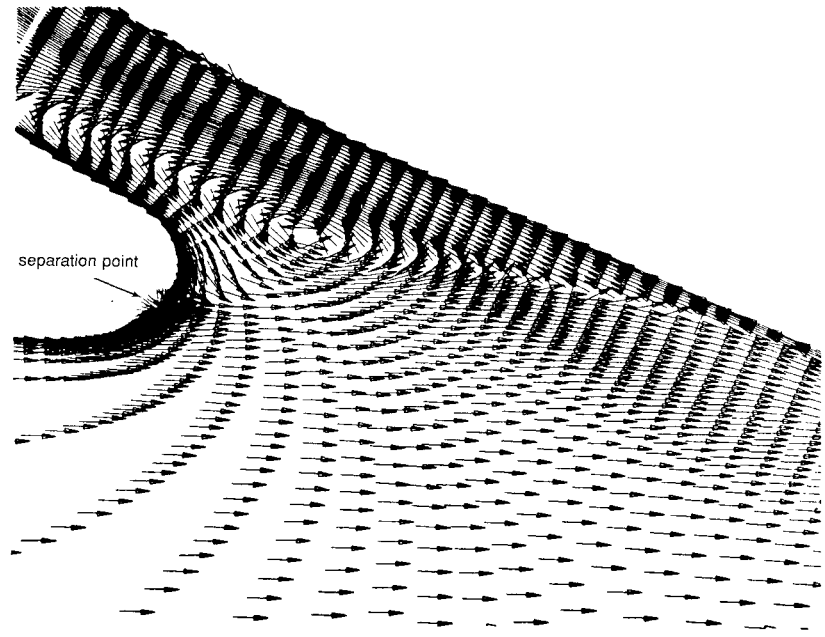

Fig. 17 Flow-direction plot in expanded portion of the "neck" region.

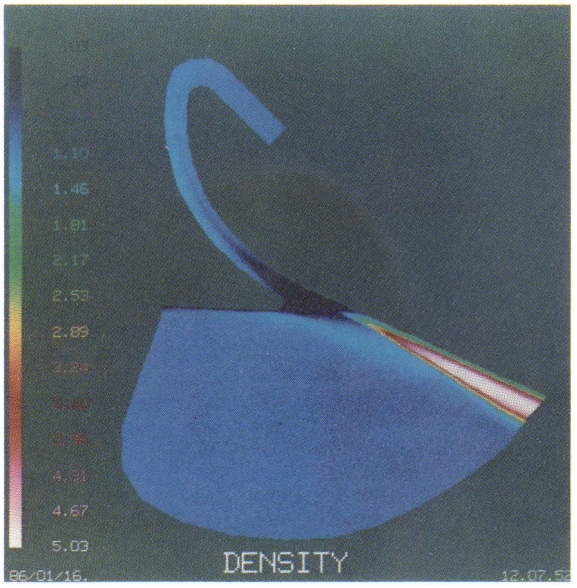

Fig. 18 Density plot of the wing-elevon cove.

Fig. 20 Temperature plot of the wing-elevon cove.

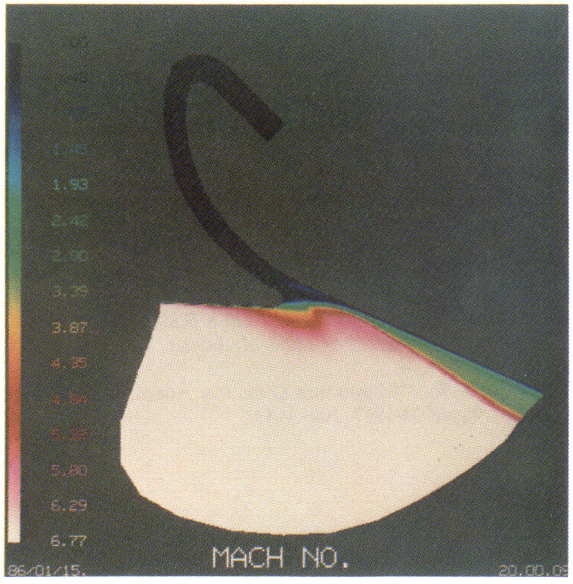

Fig. 19 Mach number plot of the wing-elevon cove.

Fig. 21 Enthalpy plot of the wing-elevon cove.

the elevon surface. Numerical values of C_p are higher than experimental data. The prediction of the slope for the steep C_p rise is higher than the experiment. This rise occurs where the shear layer merges with the shock. The occurrence of transition in this separated shear layer is likely to influence the value of this gradient. Experimental results for this test case[9] indicate heat-transfer data on the elevon to be within a factor of 2 of fully turbulent flow as calculated by a reference enthalpy method, thus suggesting the likelihood that this separated shear layer is, indeed, in transition. It should be noted that a similar effect might occur if the experimental boundary layer was substantially thicker than the one assumed in this analysis; the lower velocity might cause lower pressure recovery on the elevon and increase the distance before the inviscid level is obtained.

The value of the C_p (i.e., pressure) plateau on the elevon is within a few percent of the experimental value verifying proper post-shock inviscid conditions in the numerical model. The dip in C_p at approximately 5.45 is at the attachment point. There are not enough experimental data points to plot a profile in this section.

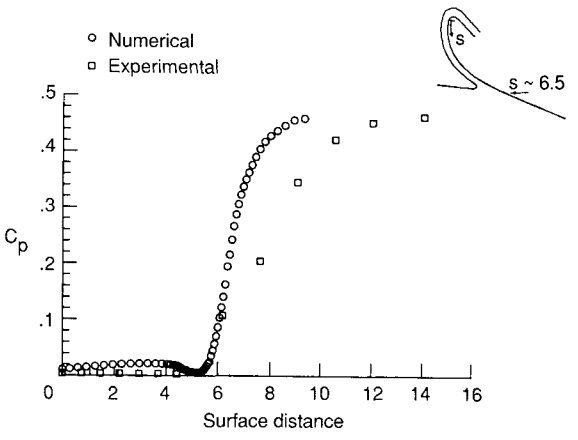

Fig. 22 Calculated and experimental pressures for the wing-elevon cove.

Conclusions

Two aerothermal flow problems of relevance in hypersonic-flow research have been modeled by compressible Navier-Stokes calculations using an ADI scheme and compared with experiment. A numerical model of the GJNT at zero angle of attack compared favorably with experimental pressures, shock standoff, and qualitative features. However, experimental heating rates beyond the recirculation zone were much higher than the numerical heating rates. Differences in the gas jet temperature were shown to be insufficient in the numerical model to account for the large discrepancy in the comparison. However, the numerical model is laminar and the heating rates from the experiment may be dominated by turbulent mixing of the incoming hot gas with the turbulent gas jet. The considerably lower heating rates in the numerical model suggest that maintaining the jet as laminar as possible might greatly enhance its cooling effectiveness.

Preliminary results from numerically modeling a wing-elevon cove indicate good agreement with experimental values of C_p and qualitative flow features. An overprediction by the numerical model in the magnitude of a steep C_p gradient occurring in the vicinity of the separated shear layer may be due to transition effects in the experimental model, since experimental results indicate heat-transfer data on the elevon to be within a factor of 2 of fully turbulent flow. In addition, numerical inflow conditions were approximations to the conditions present in the experimental model; the effect of proper inflow condition requires further assessment. However, the value of the C_p plateau after its steep rise, predicted by the numerical model, is within a few percent of the experimental value verifying the proper post-shock inviscid conditions in the numerical model. Agreement with experimental data in both cases would be greatly enhanced by including turbulence and real-gas effects in the numerical model.

Acknowledgments

The author wishes to thank Dr. C. L. Streett of the Theoretical Aerodynamics Branch at NASA Langley for helpful discussions during the course of this work. Special thanks are also given to Dr. G. Erlebacher of the Computational Methods Branch at NASA Langley for generating the grid used to solve the wing-elevon cove flowfield.

References

[1]Gardner, J. E. and Dixon, S. C., "Loads and Aeroelasticity Division Research and Technology Accomplishments for FY 1983 and Plans for FY 1984," NASA TM-85740, June 1984.

[2]Beam, R. M. and Warming, R. F., "An Implicit Factored Scheme for the Compressible Navier-Stokes Equations," *AIAA Journal*, Vol. 16, April 1976, pp. 393–402.

[3]Jameson, A., Schmidt, W., and Turkel, E, "Numerical Solution of the Euler Equations by Finite Volume Methods Using Runge-Kutta Time-Stepping Schemes," Presented at the AIAA 14th Fluid and Plasma Dynamics Conf., June 1981.

[4]Nowak, R. J., "Gas Jet and Tangent Slot Film Cooling Tests of a 12.5° Cone at Mach 6.7," NASA TP-2786, April 1988.

[5]Puster, R. L., Aerothermal Loads Branch, Loads and Aeroelasticity Div., NASA Langley Research Center, private communication, 1986.

[6]Wieting, A. R., Walsh, J. L., and Bey, K. S., "Aerothermal Environment in Control Surface Gaps in Hypersonic Flow—An Overview," AIAA Paper 83-1483, June, 1983.

[7]Bey, K. S., "Analytical Prediction of Aerothermal Environment in a Wing-Elevon Cove," NASA TM-85711, Nov. 1983.

[8]Bey, K. S., Thornton, E. A., Dechaumphai, P., and Ramakrishnan, R., "A New Finite Element Approach for Predictions of Aerothermal Loads—Progress in Inviscid Flow Computations," *Proceedings of the AIAA Computational Fluid Dynamics Conference*, AIAA, New York, July 1985.

[9]Deveikis, W. D., "Effects of Flow Separation and Cove Leakage on Pressure and Heat-Transfer Distributions Along a Wing-Cove-Elevon Configuration at Mach 6.9," NASA TP-2127, July 1983.

[10]Kutler, P., Chakravarthy, S. R., and Lombard, C. K., "Supersonic Flow Over Ablated Nosetips Using an Unsteady Implicit Numerical, Implicit Numerical Procedure," AIAA Paper 78-213, Jan. 1978.

[11]Macaraeg, M. G., "Applications of CFD to Aerothermal Heating Problems," AIAA Paper 86-0232, Jan. 1986.

[12]"Equations, Tables, and Charts for Compressible Flow," NACA Rept. 1135, Ames Research Staff, June 1953.

[13]Nowak, R. J., Albertson, C. W., and Hunt, L. R., "Aerothermal Tests of a 12.5 Cone at Mach 6.7 for Various Reynolds Numbers, Angles of Attack, and Nose Shapes," NASA TP-2345, Jan. 1983.

[14]Finley, P. J., "The Flow of a Jet from a Body Opposing a Supersonic Free Stream," *Journal of Fluid Mechanics*, Vol. 26, Pt. 2, May 1966.

[15]Eiseman, P. R., "Alternating Direction Adaptive Grid Generation," AIAA Paper 83-1937, July 1983.